Available online at www.sciencedirect.com

SciVerse ScienceDirect

Ceramics International 38 (2012) 3667–3672

CERAMICS INTERNATIONAL

www.elsevier.com/locate/ceramint

# Low-temperature combustion synthesis of nanocrystalline $HoFeO_3$ powders via a sol–gel method using glycin

Linwen Jiang [a,b], Weiliang Liu [a,*], Anhua Wu [b], Jun Xu [b], Qian Liu [b], Guoxing Qian [b], Huaijin Zhang [c]

[a] Department of Materials, Jingdezhen Ceramic Institute, Jingdezhen 333001, PR China
[b] Shanghai Institute of Ceramics, Chinese Academy of Sciences, Shanghai 200050, PR China
[c] State Key laboratory of Crystal Material, Shandong University, Jinan 250100, PR China

Received 19 August 2011; received in revised form 2 January 2012; accepted 4 January 2012
Available online 14 January 2012

**Abstract**

Single phase nanocrystalline $HoFeO_3$ powders were successfully synthesized by the sol–gel self-propagation combustion method using glycin ($C_2H_5NO_2$) as the chelating reagent at a low combustion temperature. Four different mole ratios of glycin to metal nitrate (G/M) were used to prepare $HoFeO_3$ powders in the experiment. The XRD patterns indicate monophasic $HoFeO_3$ powders can be formed by further calcination, the SEM micrographs show that the nano-sized grains with distinguishable boundaries had been obtained. The *M–H* curves show $HoFeO_3$ powders had the characteristic of antiferromagnetism at 50 K, while the powders had the characteristic of paramagnetism as the ambient temperature reached 100 K or 300 K. The FC/ZFC magnetic measurement results demonstrate that there was a transition from antiferromagnetism to paramagnetism in $HoFeO_3$ nanopowders as the temperature was increased.


*Keywords:* $HoFeO_3$; G/M; Phase forming; Magnetic properties

## 1. Introduction

In recent years, the orthorhombic perovskite-type $RFeO_3$ (where R stands for rare-earth element) materials have attracted considerable interest due to their excellent magnetic properties [1–3]. Those materials have wide applications in various fields, such as fuel cells [4], catalysts [5], sensors [6] and environmental monitoring [7]. It is important to develop techniques to produce $RFeO_3$ powders with controlled composition and size since the ultrafine and ultrapure $RFeO_3$ powders usually exhibit superior properties, such as large surface area, higher chemical reactivity [8]. The conventional solid state reaction method of preparing $RFeO_3$ powders is a tedious process requiring a very high sintering temperature, and obtaining large-size even agglomerated powders. Wet chemical methods have been reported widely for preparing ultrafine and ultrapure $RFeO_3$ powders, such as hydrothermal synthesis [9], sol–gel method [10] and coprecipitation method [11]. Among these, sol–gel method is a widely used synthesis technique, which involves atomic scale mixing and has a high reaction rate [12]. Furthermore, the sol–gel process is simple and easy to operate.

The novel sol–gel auto-combustion technique using glycin as chelating reagent has been used to prepare highly active, homogeneous and stoichiometric $HoFeO_3$ nanopowders in the paper. The chelate reagent glycin, which has a strong chelate ability to metallic cations [13], was expected to lower the temperature of gel burning and reduce the amount of residual organic compounds in the as-burnt powders due to its smaller molecular weight than other chelating reagents, such as citric acid, polyvinyl alcohol (PVA), stearic acid and hydrazine compounds [14–16]. Excitedly, the combustion temperature of gels with glycin is low to 200 °C, and it will be beneficial for obtaining stoichiometric $HoFeO_3$ nanopowders. In this paper, we report the low-temperature combustion synthesis of nanocrystalline $HoFeO_3$ powders via a sol–gel method using glycin. The effects of different mole ratios of glycin to metal nitrate (G/M) on the phase forming and morphology feature of

* Corresponding author. Tel.: +86 21 52414238; fax: +86 21 52413903.
*E-mail address:* us.gs@163.com (W. Liu).

0272-8842/$36.00 
doi:10.1016/j.ceramint.2012.01.007

synthesis products were studied. In addition, the magnetic properties of prepared $HoFeO_3$ nanopowders were also investigated.

## 2. Experimental

$Ho_2O_3$ (99.99% purity), $Fe(NO_3)_3{\cdot}9H_2O$ (98.5% purity) and glycin ($C_2H_5NO_2$, AR) were used as raw materials to prepare $HoFeO_3$. $Ho_2O_3$ was dissolved in nitric acid forming $Ho(NO_3)_3$ solutions by heating and stirring using a magnetic agitator. $Fe(NO_3)_3{\cdot}9H_2O$ was dissolved in distilled water and mixed with $Ho(NO_3)_3$ in the stoichiometric ratio of Ho:Fe = 1:1. Glycin was then added as a chelating reagent to the above solutions, in order to investigate the effect of glycin content on the powder synthesis, four different G/M values were used to prepare $HoFeO_3$ powders. The mixed solutions were continuously stirred using a magnetic agitator until sticky gels were formed. The obtained gels were removed into a big alumina crucible to process combustion experiments. The gels got burnt in a self-propagating combustion manner at a presetting temperature 300 °C in an open furnace, and voluminous porous powders were formed following along with plenty of brown fumes escaping from alumina crucible. Finally the as-burnt powders were calcined at different temperatures for 3 h.

Thermogravimetry (TG) and differential thermal analysis (DTA) in the temperature range of 25–700 °C were used to monitor the decomposition of the precursors using a NETZSCH STA 449C at a heating rate of 10 °C/min. Phase identification was checked by powder X-ray diffraction (XRD, D/Max-2550 V, Rigaku, Japan) using Cu Kα radiation and nickel as the filter at a scan rate of 12°/min from 10° to 80° (2$\theta$), and phases were identified by using Jade5 analysis software. Microstructure analysis was performed by a scanning electron microscope (SEM, JSM-6700F). The grain sizes of the powders were estimated following the Scherrer's equation. The magnetic measurements of the samples were performed on a superconducting quantum interference device magnetometer (Quantum design, PPMS-9).

## 3. Results and discussion

The chelating reagent glycin has a moderate flammability and can be ignited immediately during heat treatment at about 300 °C. It was noted that the thermal decomposition temperature of gels started at about 200 °C, while the gels and crucibles had a drastic endothermic procedure before gels got burnt, the real presetting temperature 300 °C was higher than the nominal decomposition temperature 200 °C. The combustion process can be considered as a redox reaction occurring between the amino-carboxyl groups acting as reductants and $NO_3^-$ ions acting as oxidants. The burning instantaneously propagated when the gels reached the redox reaction temperature, and finally formed a large volume of loose powders with plenty of microscopic pores. The combustion results show that all of the gel samples prepared with different G/M values exhibited self-propagating combustion behaviors. Fig. 1 shows the SEM micrograph of as-burnt

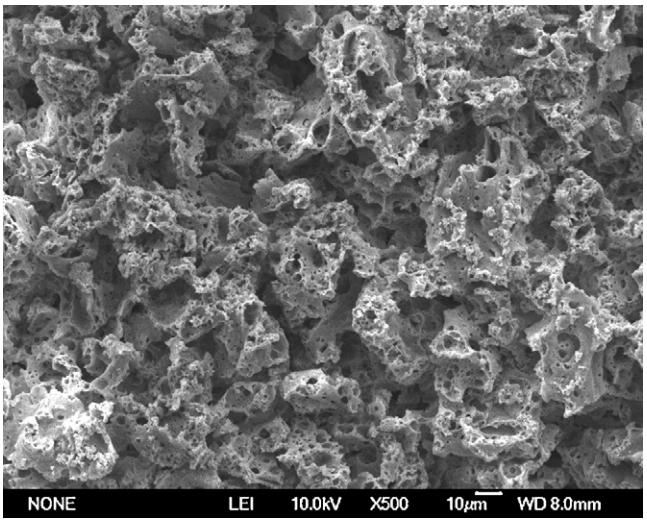


Fig. 1. Scanning electron microscope (SEM) micrograph of the as-burnt powders prepared with G/M = 0.5.

powders prepared with G/M = 0.5. It was observed that the porous powders with continuous network were formed. The puffy structure and plenty of tiny pores were due to the large amount of escaping gases during combustion [17,18].

The combined TG and DTA curves of the gels derived from different G/M values are shown in Figs. 2 and 3. For Fig. 2, we can observe that an overall weight of 66% was reduced during thermal decomposition. There was a low endothermic peak at about 79 °C, which was due to the removal of water in the gel. As the temperature was increased, the water in the gel evaporated faster, and another biggest endothermic peak was observed at about 157 °C. The sharp exothermic peak at about 200 °C with a large weight loss of about 45% can be attributed to the redox reaction occurring between glycin and metal nitrates. The remaining weight loss occurring in some small steps corresponded to the slow burning of incombustible matters in the region of 250–350 °C. Typically, the weak peak at about 340 °C indicates that the burning of organic residues

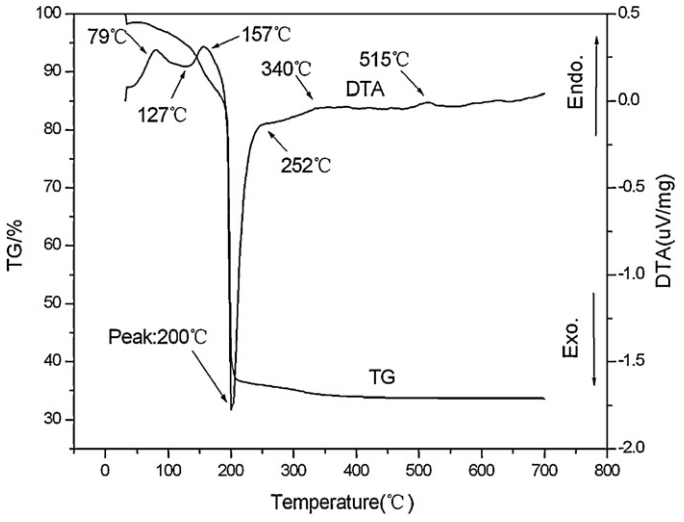


Fig. 2. Combined DTA and TG plots of the gel sample prepared with G/M = 1.

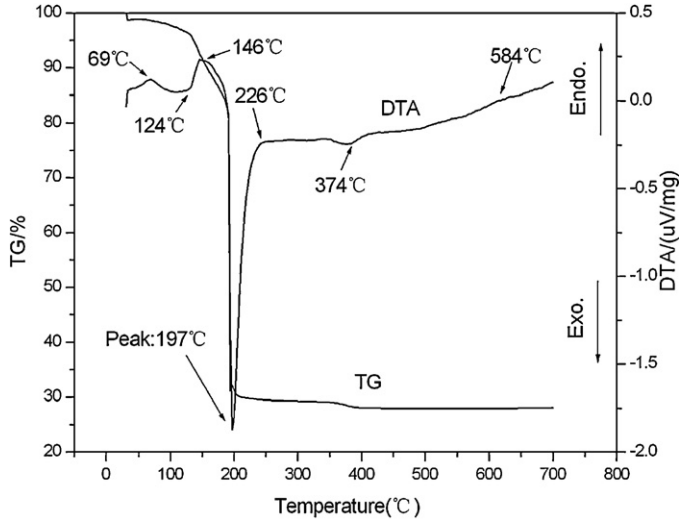


Fig. 3. Combined DTA and TG plots of the gel sample prepared with G/M = 1.5.

remained happening in the precursors [17–19]. The decomposition of residual organics became weaker and weaker as the temperature was increased and the weight loss is extremely low. The TG and DTA curves of gel prepared with G/M = 1.5 are shown in Fig. 3. Compare with Fig. 2, the gel had a lower decomposition temperature 197 °C and higher total weight loss of 72%, though, both of them had a similar variety tendency of heat values and weight loss.

The influence of different G/M values on the $HoFeO_3$ powders synthesis is shown in Table 1, the prepared products with G/M = 0.5 and 1 had the typical color of organics, where the brown or black color indicates that residual organics coexisted in the as-burnt powders. The products prepared with G/M = 1.5 and 2 with the feature of high-density and large-size show that a relatively drastic redox reaction had occurred during combustion. The effect of different calcination temperatures on the powder synthesis is also indicated by the contrast of product color, the powders calcined at 800 °C or 1000 °C with pure yellow color show that the organics had been almost burnt out during calcination.

The effects of different G/M values on the powder synthesis can be indicated exactly from the XRD patterns. Fig. 4 shows the XRD patterns of the as-burnt powders with different G/M values, the as-burnt powders with G/M = 0.5 or 1 with an

Table 1
Comparison of auto-combustion synthesis products prepared with different G/M values and calcination temperatures.

| G/M values | Calcination temperature of raw products | Final products |
|---|---|---|
| 0.5:1 | No calcination | Puffy brown powders |
| 1:1 | No calcination | Puffy brown powders |
| 1:1 | Keeping 800 °C for 3 h | Puffy yellow powders |
| 1:1 | Keeping 1000 °C for 3 h | Puffy yellow powders |
| 1.5:1 | No calcination | Brown high-density powders |
| 2:1 | No calcination | Black high-density powders with large grains |

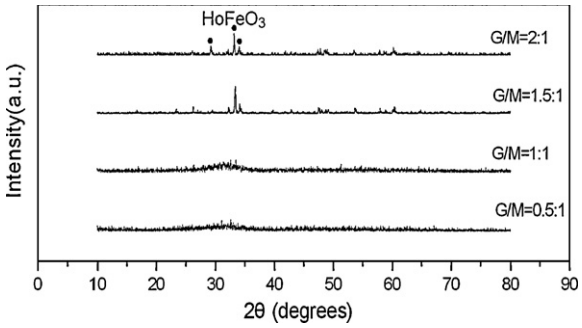


Fig. 4. XRD patterns of the as-burnt powders prepared with different G/M values.

amorphous structure instead of crystalline $HoFeO_3$ structure suggests the powders had not been crystallized during combustion processing. Comparatively, the XRD patterns with G/M value = 1 or 1.5 show the $HoFeO_3$ phase had been formed partially during the combustion processing. Therefore, we can conclude that the higher G/M values were in favor of the crystallization of $HoFeO_3$ powders, while the combustion reaction of high G/M values was so drastic that some other impure phases may coexist in the prepared powders during combustion [16–18,20]. Fig. 5 shows the XRD patterns of as-burnt powders calcined at 800 °C and 1000 °C, it is clearly seen that the monophasic $HoFeO_3$ powders calcined at 800 °C and 1000 °C had been formed.

The average crystallite sizes of synthesized powders were calculated using the X-ray broadening of the (1 1 2) diffraction peak by the well-known Scherrer equation [17,21,22].

$$D = \frac{0.89\lambda}{\beta \cos\theta}$$

where $D$ is crystallite size in nm, $\lambda$ is the radiation wave length (0.15405 nm for Cu Kα), $\beta$ is the corrected full width at half maximum and $\theta$ is the diffraction angle. According to the XRD results of powders calcined at 800 °C and 1000 °C in Fig. 5, it can be calculated that the crystallite sizes of $HoFeO_3$ samples calcined at 800 °C and 1000 °C were 36.6 nm and 38.2 nm, respectively. As expected, the crystallite size increased slightly as the calcination temperature was increased.

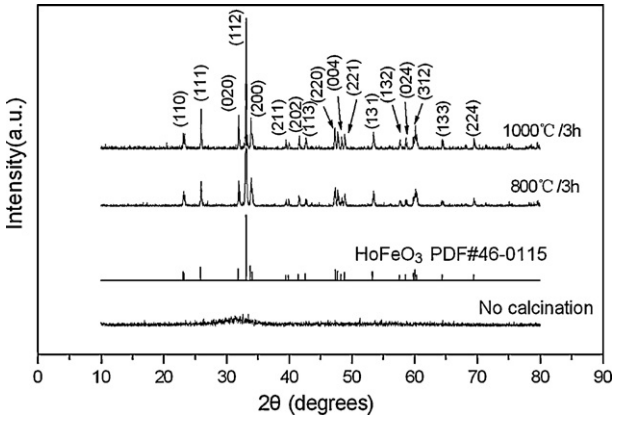


Fig. 5. XRD patterns of the powders prepared with G/M = 1:1 and calcined at different temperatures.

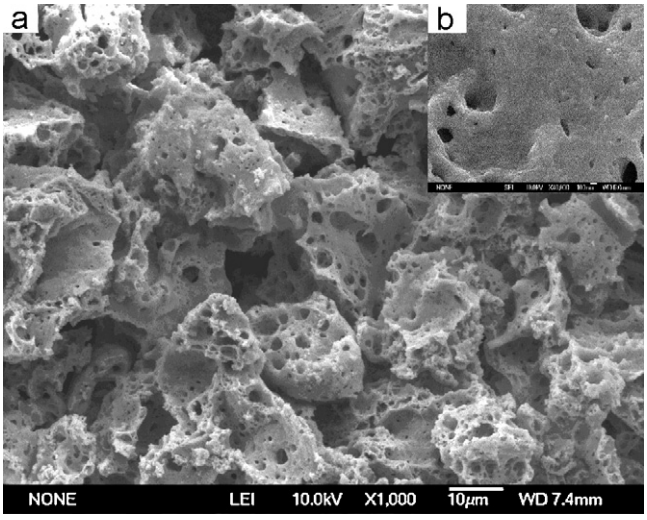


Fig. 6. SEM micrograph of as-burnt powders prepared with G/M = 1: (a) 1000×, (b) 40,000×.

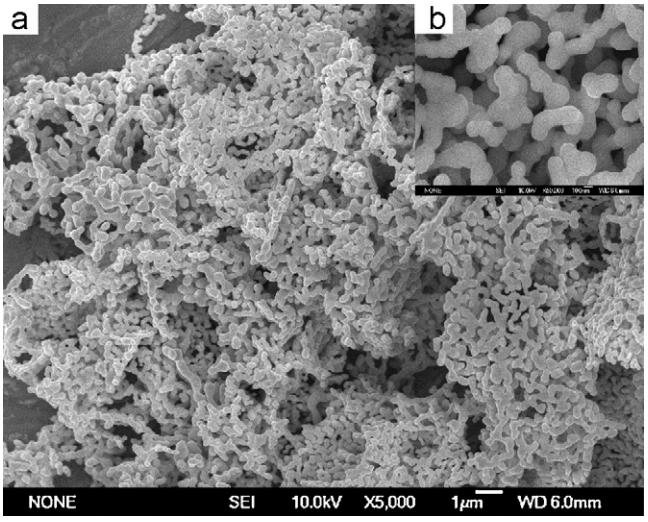


Fig. 8. SEM micrograph of powders prepared with G/M = 1 and calcined at 1000 °C: (a) 5000× (b) 50,000×.

Figs. 6–8 show the SEM figures of powders without calcination, calcined at 800 °C and 1000 °C, respectively. It was clearly seen that the powders without calcination had network-like structure, which was just like honeycomb. The powders calcined at 800 °C and 1000 °C appeared to be round grains with distinguishable boundaries. From Figs. 7(b) and 8(b), it can be observed that the grain sizes were about in the region of 100–300 nm. In the XRD discussing part, we have known the crystallite size was about 36 nm, it indicates the grains may contain 3–8 crystallites. It is an interesting phenomenon that the powders calcined at a high temperature had smaller sizes and more distinguishable boundaries than those calcined at a low temperature. It may include the below three reasons: (1) the calcination temperature at 800 °C or 1000 °C in the experiment would not lead to an extensive grain agglomeration since the sintering temperature of $HoFeO_3$ powders is higher than 1300 °C. (2) Single grain usually contained a few crystallites, and those crystallites in single grain were not the most closed-packed. As the calcination temperature was increased, the activity of crystallites in single grain became stronger; the bulk was reduced as a result of the more closed-packed crystallites. Therefore, the single grain presented smaller sizes at high temperatures. (3) Some incombustible matters in the $HoFeO_3$ grains which did not get away from powders during calcination made the $HoFeO_3$ grains present bigger sizes. A higher temperature can minimize the content of residual incombustible matters [16,18], and make the grains present smaller sizes and more distinguishable boundaries.

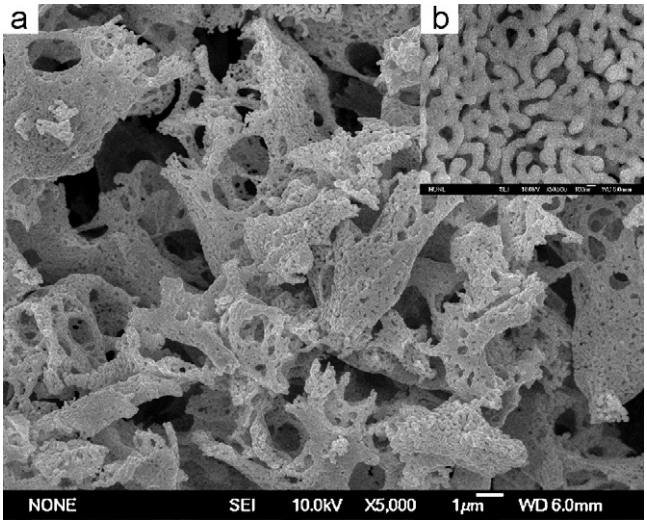


Fig. 7. SEM micrograph of powders prepared with G/M = 1 and calcined at 800 °C: (a) 5000×, (b) 50,000×.

The orthoferrite $HoFeO_3$ crystallizes in a distorted perovskite structure with an orthorhombic unit cell. Ho and iron atoms belong to different groups of transition elements (4f and 3d, respectively) with different magnetic moment values. The magnetic moments of iron and Ho atoms as well as the interactions between them are the source of magnetic properties of $HoFeO_3$ [23]. Fig. 9(a) shows the hysteresis loop of $HoFeO_3$ samples at 50 K. The magnetization versus magnetic field ($M$–$H$) curve displayed hysteretic loop, the shape of the loop was just the characteristic of antiferromagnetism, the saturation magnetization ($M_s$) reached 5.14 emu/g and an exchange bias field of 590 Oe in the negative direction was obtained. The high $M_s$ is believed that the exchange coupling effect arises because of the presence of an antiferromagnetic layer at the surfaces of the $HoFeO_3$ nanopowders [15]. Moreover, in nanopowders, uncompensated surface or grain boundaries ordering of the spins are known to create interfacial exchange energy with the core particles [24]. It can be observed that the hysteresis loop is shifted slightly along the field axis, loop is highly asymmetrical. Such a shift is an indication for the exchange interaction between different magnetic sublattices. One reasonable explanation is the coupling exchange interaction between Fe sublattices and Ho sublattices [13].

Fig. 9(b) shows the hysteresis loop at 100 K. Different from the magnetic properties at 50 K, the magnetization versus

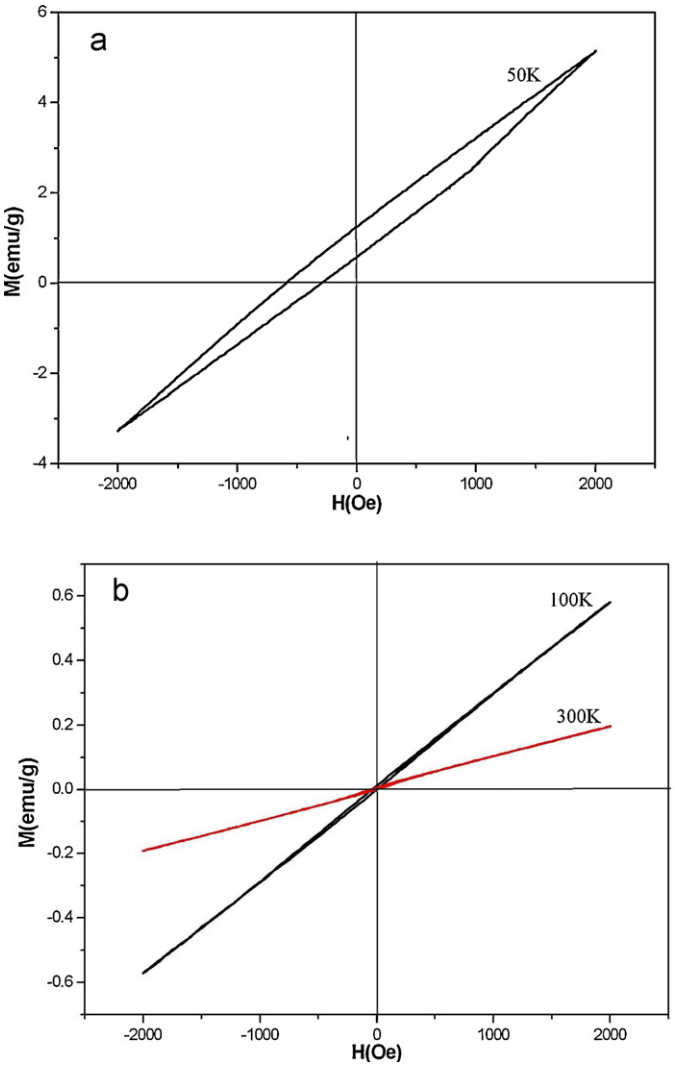


Fig. 9. Magnetization versus magnetic field hysteresis loops for $HoFeO_3$ samples prepared with G/M = 1 at different temperatures: (a) 50 K, (b) 100 K and 300 K.

magnetic field (*M–H*) curve displayed linear loop, the shape of the loop displayed typical characteristic of paramagnetism, and the magnetization still had an identical tendency to increase even at a field of 2000 Oe. The rapid decreasing of material antiferromagnetism at 100k was attributed to the thermal fluctuations that changed the main antiferromagnetic ordering of the spins. In $HoFeO_3$ nanoparticles, it is believed that the magnetic moments of the distorted $FeO_6$ octahedra are the main source of the magnetic properties due to the strong exchange interaction between Fe sublattices [23], and the spontaneous magnetization became weak even disappeared as the ambient temperature was increased. Fig. 9(b) shows the other hysteresis loop at 300 K, similar with the magnetic properties at 100 K, the magnetization versus magnetic field (*M–H*) curve also displayed linear loop, the different point is that the $HoFeO_3$ nanoparticles at 300 K had lower magnetic susceptibility than that of 100 K. When ambient temperature exceeds Curie temperature, the relation

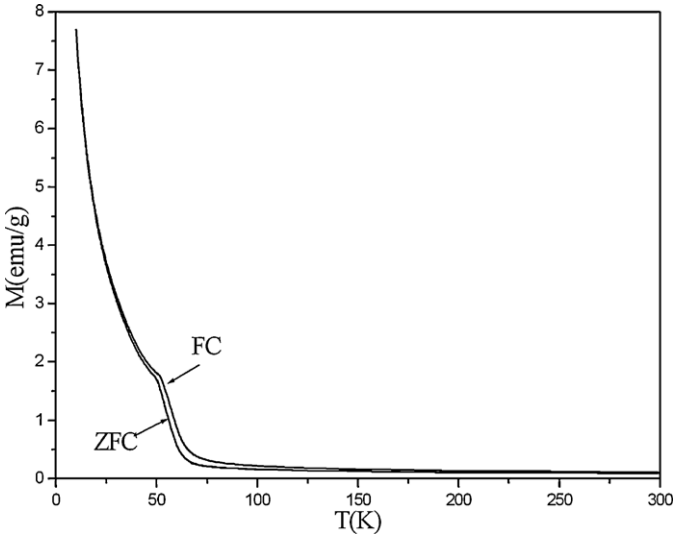


Fig. 10. Temperature dependence of the magnetization after ZFC and FC for $HoFeO_3$ samples prepared with G/M = 1 and calcined at 1000 °C.

between magnetic susceptibility and temperature obeys Curie–Weiss law [8,25].

$$\chi = \frac{C}{T - Tc}$$

where $\chi$ is magnetic susceptibility, $C$ is Curie constant, $T$ is ambient temperature, $T_c$ is Curie temperature. According to the law, it can be known that magnetic susceptibility will decrease as the ambient temperature was increased.

The magnetization as a function of temperature under zero-field-cooled (ZFC) and field-cooled (FC) modes at an applied field of 100 Oe is shown in Fig. 10. The shape of *M–T* curve indicates that the magnetization of $HoFeO_3$ can be described as the magnetization sum of two terms. One term (mainly) is due to the antiferromagnetism of distorted $FeO_6$ octahedra [23], and the other term is attributable to the paramagnetism of Ho sublattices. The magnetic measurement results show that there was a transition from antiferromagnetism to paramagnetism in $HoFeO_3$ nanopowders as the temperature was increased. When the ambient temperature was low, the antiferromagnetism contribution was dominant as it is believed that the magnetic moments of the distorted $FeO_6$ octahedra are the main source of magnetic properties [23]. As the ambient temperature was increased, the antiferromagnetism decreased rapidly, and the paramagnetism contribution of Ho ions became dominant.

## 4. Conclusions

Monophasic and nano-sized $HoFeO_3$ powders were synthesized successfully by using glycin-assisted sol–gel combustion method at a low combustion temperature. The results suggest the G/M values of precursors had a significant influence on the phase forming and morphology feature of synthesis products. High G/M values were in favor of crystallization of $HoFeO_3$ powders, while the amorphous structure had not been eliminated completely. The $HoFeO_3$ nanopowders had the feature of antiferromagnetism when the ambient temperature

was 50 K. As the temperature was increased, the linear loop displayed the characteristic of paramagnetism. The FC/ZFC magnetic measurement results demonstrate that there was a transition from antiferromagnetism to paramagnetism in $HoFeO_3$ nanopowders as the temperature was increased.

## Acknowledgements

The authors would like to acknowledge the financial support from National Natural Science Foundations of China (Grant Nos. 50932003 and 51002097). This work is also supported by the Opening Project of State Key laboratory of Crystal Material (Grant No. KF1006).

## References

[1] Y.S. Didosyan, H. Hauser, H. Wolfmayer, J. Nicolics, P. Fulmek, Magneto-optical rotational speed sensor, Sens. Actuators A 106 (2003) 168–171.
[2] S. Mathur, M. Veith, R. Rapalaviciute, H. Shen, G.F. Goya, W.L. Martins Filho, T.S. Berquo, Molecule derived synthesis of nanocrystalline $YFeO_3$ and investigations on its weak ferromagnetic behavior, Chem. Mater. 16 (2004) 1906–1913.
[3] D.S. Schmool, N. Keller, M. Guyot, R. Krishnan, M. Tessier, Evidence of very high coercive fields in orthoferrite phases of PLD grown thin films, J. Magn. Magn. Mater. 195 (1999) 291–298.
[4] N.Q. Mih, Ceramic Fuel-Cells, J. Am. Ceram. Soc. 76 (1993) 563–588.
[5] S. Bai, X. Fu, J. Wang, Q. Yang, Y. Sun, S. Zeng, Photocatalytic activity of $LaFeO_3$, Chin. J. Appl. Chem. 17 (2000) 343–345.
[6] Y. Shimizu, M. Shimabukuro, H. Arai, T. Seiyama, Enhancement of humidity sensitivity for perovskite-type oxides having semiconductivity, Chem. Lett. 163 (1985) 917–920.
[7] G. Martinelli, M.C. Carotta, M. Ferroni, Y. Sadaoka, E. Traversa, Screen-printed perovskite-type thick films as gas sensors for environmental monitoring, Sens. Actuators B 55 (1999) 99–110.
[8] S. Mathur, H. Shen, N. Lecerf, A. Kjekshus, H. Fjellvag, G.F. Goya, Nanocrystalline orthoferrite $GdFeO_3$ from a novel heterobimetallic precursor, Adv. Mater. 14 (2002) 1405–1409.
[9] W.J. Zheng, R.H. Liu, D.K. Peng, G.Y. Meng, Hydrothermal synthesis of $LaFeO_3$ under carbonate-containing medium, Mater. Lett. 43 (2000) 19–22.
[10] Q. Ming, M.D. Nersesyan, A. wagner, J. Ritchie, J.T. Richardson, D. Luss, A.J. Jacobson, Y.L. Yang, Combustion synthesis and characterization of Sr and Ga doped $LaFeO_3$, Solid State Ionics 122 (1999) 113–121.
[11] S. Nakayama, $LaFeO_3$ perovskite-type oxide prepared by oxide-mixing, co-precipitation and complex synthesis methods, J. Mater. Sci. 36 (2001) 5643–5648.
[12] M. Pal, D. Chakravorty, Synthesis of nanocrystalline yttrium iron garnet by sol–gel route, Physica E 5 (2000) 200–203.
[13] V. Bedekar, O.D. Jayakumar, J. Manjunna, A.K. Tyagi, Synthesis and magnetic studies of nano-crystalline $GdFeO_3$, Matter. Lett. 62 (2008) 3793–3795.
[14] M. Ari, K.J. Miller, B.A. Marinkovic, P.M. Jardim, R.D. Avillez, F. Rizzo, M.A. White, Rapid synthesis of the low thermal expansion phase of $Al_2Mo_3O_{12}$ via a sol–gel method using polyvinyl alcohol, J. Sol–Gel Sci. Technol. 58 (2011) 121–125.
[15] R. Maiti, S. Basu, D. Chakravorty, Synthesis of nanocrystalline $YFeO_3$ and its magnetic properties, J. Magn. Magn. Mater. 321 (2009) 3274–3277.
[16] J.S. Feng, T. Liu, Y.B. Xu, J.Y. Zhao, Y.Y. He, Effect of PVA content on the synthesis of $LaFeO_3$ via sol–gel route, Ceram. Int. 37 (2011) 1203–1207.
[17] S.H. Vajargah, H.R. Madaah Hosseini, Z.A. Nemati, Preparation and characterization of yttrium iron garnet (YIG) nanocrystalline powders by auto-combustion of nitrate–citrate gel, J. Alloy Compd. 430 (2007) 339–343.
[18] X.Z. Guo, B.G. Ravi, P.S. Devi, J.C. Hanson, J. Margolies, R.J. Gambino, J.B. Parise, S. Sampath, Synthesis of yttrium iron garnet (YIG) by citrate-nitrate gel combustion and precursor plasma spray processes, J. Magn. Magn. Mater. 295 (2005) 145–154.
[19] X.W. Qi, J. Zhou, Z.X. Yue, Z.L. Gui, L.T. Li, Auto-combustion synthesis of nanocrystalline $LaFeO_3$, Mater. Chem. Phys. 78 (2002) 25–29.
[20] H. Shen, G.F. Cheng, A.H. Wu, J.Y. Xu, J.T. Zhao, Combustion synthesis and characterization of nano-crystalline $LaFeO_3$ powder, Phys. Stat. Sol. A 206 (2009) 1420–1424.
[21] C.S. Kuroda, T. Taniyama, Y. Kitamoto, Y. Yamazaki, Magneto-optical properties and morphology of particulate film consisting of Bi-YIG coprecipitated particles, J. Magn. Magn. Mater. 241 (2002) 201–206.
[22] S. Taketomi, C.M. Sorensen, K.J. Klabunde, Preparation of yttrium iron–garnet nanocrystals dispersed in nanosize-pore glass, J. Magn. Magn. Mater. 222 (2000) 54–64.
[23] A. Wu, H. Shen, J. Xu, L. Jiang, L. Luo, S. Yuan, S. Cao, H. Zhang, Preparation and magnetic properties of $RFeO_3$ nanocrystalline powders, J. Sol–Gel Sci. Technol. 59 (2011) 158–163.
[24] M.S. Seehra, A. Punnoose, Particle size dependence of exchange-bias and coercivity in CuO nanoparticles, Solid State Commun. 128 (2003) 299–302.
[25] Z. Guan, Z. Zhang, J. Jiao, Physical Properties of Inorganic Materials, Tsinghua University Press, Beijing, 2006.